In silico ADMET and molecular docking study on searching potential inhibitors from limonoids and triterpenoids for COVID-19

Seshu Vardhan, Suban K. Sahoo[*]

Department of Applied Chemistry, S.V. National Institute of Technology (SVNIT), Surat, 395007, Gujarat, India

ARTICLE INFO

ABSTRACT

Virtual screening of phytochemicals was performed through molecular docking, simulations, in silico ADMET and drug-likeness prediction to identify the potential hits that can inhibit the effects of SARS-CoV-2. Considering the published literature on medicinal importance, 154 phytochemicals with analogous structure from limonoids and triterpenoids were selected to search potential inhibitors for the five therapeutic protein targets of SARS-CoV-2, i. e., 3CLpro (main protease), PLpro (papain-like protease), SGp-RBD (spike glycoprotein-receptor binding domain), RdRp (RNA dependent RNA polymerase) and ACE2 (angiotensin-converting enzyme 2). The in silico computational results revealed that the phytochemicals such as glycyrrhizic acid, limonin, 7-deacetyl-7-benzoyl-gedunin, maslinic acid, corosolic acid, obacunone and ursolic acid were found to be effective against the target proteins of SARS-CoV-2. The protein-ligand interaction study revealed that these phytochemicals bind with the amino acid residues at the active site of the target proteins. Therefore, the core structure of these potential hits can be used for further lead optimization to design drugs for SARS-CoV-2. Also, the medicinal plants containing these phytochemicals like licorice, neem, tulsi, citrus and olives can be used to formulate suitable therapeutic approaches in traditional medicines.

1. Introduction

There is extensive ongoing research globally to formulate suitable therapeutic approaches to control the effects of the severe acute respiratory syndrome coronavirus 2 (SARS-CoV-2) to human life that caused the disease COVID-19. The first patient infected with SARS-CoV-2 was detected in December 2019 at Wuhan, China [1]. Subsequently, the virus spread across 187 countries and territories due to its high human to human contagious nature and infected 10,710,005 as of July 3, 2020 with a total death of 517,877 [2]. The World Health Organization (WHO) declared the outbreak of SARS-CoV-2 as a public health emergency of international concern (PHEIC) on January 30, 2020, and a pandemic on March 11, 2020 [3]. The non-availability of medically proven efficacious drugs or vaccines is the main concern of the COVID-19 pandemic [4]. Therefore, effective steps like identification of the infected persons through rapid diagnosis, self-quarantine or isolation, social distancing, use of face masks and hand sanitizer, etc. are taken to fight against this pandemic. In addition, the drugs like hydroxychloroquine, remdesivir, favipiravir, arbidol, hydroxychloroquine/azithromycin, lopinavir/ritonavir and lopinavir/ritonavir combined with interferon beta, etc. are repurposed, but despite some promising results further clinical studies are required to examine their mechanisms of inhibition, efficacy and safety in the treatment of COVID-19 [5–9]. Therefore, both computational and experimental approaches are adopted to search suitable drugs from the library of FDA-approved drugs, and also drugs under clinical trial but not yet repurposed against COVID-19. Simultaneously, some recent reports supporting the use of traditional medicines as an adjuvant for the treatment of COVID-19 [10–12] and therefore, there is also continuing efforts to integrate the use of both western drugs and traditional medicines for formulating suitable therapeutic strategies.

The computational approaches like molecular dynamics simulations, molecular docking, drugs-likeness prediction, in silico ADMET study, etc. are adopted mainly to screen potential drugs/molecules from various databases/libraries. The computational screening saves the experimental cost and time in the field of drug discovery. Considering the recent results of the use of traditional medicines in managing the COVID-19 epidemic [10–12], the current research work was carried out to screen phytochemicals found mainly in the Indian medicinal plants with the important objectives: (i) to search phytochemicals that bind

Table 1

List of phytochemicals screened based on *in silico* ADMET, drug-likeness and published pharmaceutical data.

Compounds	Sources	Medicinal properties	miLogP	TPSA	Ref.
Corosolic acid	Lagerstroemia speciosa	Supress proliferation of cancer cells	5.87	77.75	[32]
Glycyrrhizic acid	Licorice	Treats liver diseases, Anti HIV-1, SARS-CoV	1.97	267.04	[33, 34]
Maslinic acid	Olives	Anti-oxidant, anti-inflammatory, weak inhibition to cytochrome P450	5.81	77.75	[35]
2-Hydroxysenganolide	Fruits of khaya senegalensis	Anti-fungal activity especially against botrytis cinerea	1.47	132.51	[36]
Oleanane	Woody angiosperms	Anti-oxidant, anti-inflammatory, hepatoprotective, cardioprotective, antipruritic, spasmolytic, anti-allergic, anti-microbial, anti-viral and anti-cancer especially against breast cancer	8.86	0	[37]
7-Deacetyl-7-benzoylgedunin	Neem (Azadirachta indica)	Activity against HL60 leukemia cells	6.07	95.35	[38]
Epoxyazadiradione	Neem (Azadirachta indica)	Plasmodium falciparum plasmepsin I inhibitor	3.66	86.11	[39]
Limonin	Citrus fruits	Inhibit the HIV-1 replication in cellular systems	2.53	104.58	[40]
7-Deacetylgedunin	Neem (Azadirachta indica)	Anti-malarial, anti-inflammatory	3.64	89.27	[41]
Oleanolic acid	Ocimum Sanctum (Basil)	Therapeutic potential for neurodegenerative diseases	6.72	57.53	[42]
Ursolic acid	Ocimum Sanctum (Basil)	Therapeutic potential for neurodegenerative diseases	6.79	57.53	[43]
Limonin glucoside	Citrus fruits	Inhibit colon adenocarcinoma cell proliferation through apoptosis	−0.29	214.96	[44]
Azadiradionolide	Neem (Azadirachta indica)	Apoptosis inducing activity	2.85	86.75	[45]
Gedunin	Neem (Azadirachta indica)	*Anti*-plasmodial	4.34	95.35	[46]
Obacunone	Citrus fruits	Represses solmonella pathogenicity and also inhibits human colon cancer	3.8	95.35	[47]

Table 2

The dock score of screened phytochemicals binding at the active site of the main protease 3CLpro and their important interactions with various amino acid residues.

Phytochemicals	B.E. (kcal/mole)	Important interactions with residues at the active site, catalytic dyad (HIS41 and CYS145) and GLU166
7-Deacetyl-7-benzoylgedunin	−9.1	Carbon hydrogen bond: GLN189; Hydrogen bond: GLU166, HIS163; VDW: ARG188, ASP187, HIS164, GLY143, SER144, LEU141, ASN142, PHE140, HIS172, LEU167; Pi-Pi T-shaped: HIS41; Alkyl: MET165; Pi-Alkyl: CYS145.
Glycyrrhizic acid	−8.7	Hydrogen bond: HIS163, PHE140, GLU166, ASP197; Carbon hydrogen bond: HIS41, GLN189, MET165; VDW: MET49, HIS164, ASP187, ARG187, ARG188, THR190, ALA191, LEU50, HIS172, SER144, LEU141, ASN142.
Limonin	−8.7	Hydrogen bond: GLU166, HIS163, CYS145; Pi-donor: GLY143; Carbon hydrogen bond: GLN189; VDW: ASN142, HIS164, HIS41, MET49.
Obacunone	−7.5	Hydrogen bond: GLU166, HIS163, CYS145; Pi-donor: GLY143; Pi-Alkyl: CYS145; VDW: MET165, GLN189, ASN142, HIS41, HIS164.

effectively at the active sites of the therapeutic protein targets of SARS-CoV-2, (ii) to propose important hits that can be further investigated for lead optimization and drug discovery, and (iii) to provide computational evidence for formulating traditional medicines against SARS-CoV-2.

Our literature survey revealed that the triterpenoids like 3β-friedelanol from *Euphorbia neriifolia,* quinone-methide triterpenoids extracted from *Tripterygium regelii* (celastraceae) and glycyrrhizin from *Glycyrrhiza glabra* are experimentally proven to inhibit the effects of SARS-CoV (first identified in Guangdong, China in 2002) [13–16]. Also, our recent molecular docking studies of phytochemicals against the therapeutic protein targets of SARS-CoV-2 supported the effective binding affinity with limonin, a triterpenoid found in citrus [17]. The highest level of genomic similarity between SARS-CoV and SARS-CoV-2 [18], and the

effectiveness of triterpenoids against SARS-CoV prompted us to search potential phytochemicals from limonoids and triterpenoids. In this manuscript, 154 phytochemicals from limonoids and triterpenoids were selected by considering their known medicinal importance to search potential hits for the five therapeutic protein targets of SARS-CoV-2, i.e., 3CLpro (main protease), PLpro (papain-like protease), SGp-RBD (spike glycoprotein-receptor binding domain), RdRp (RNA dependent RNA polymerase) and ACE2 (angiotensin-converting enzyme 2). The phytochemicals were screened through *in silico* molecular docking, simulations, ADMET and drugs-likeness prediction to propose the potential hits against SARS-CoV-2.
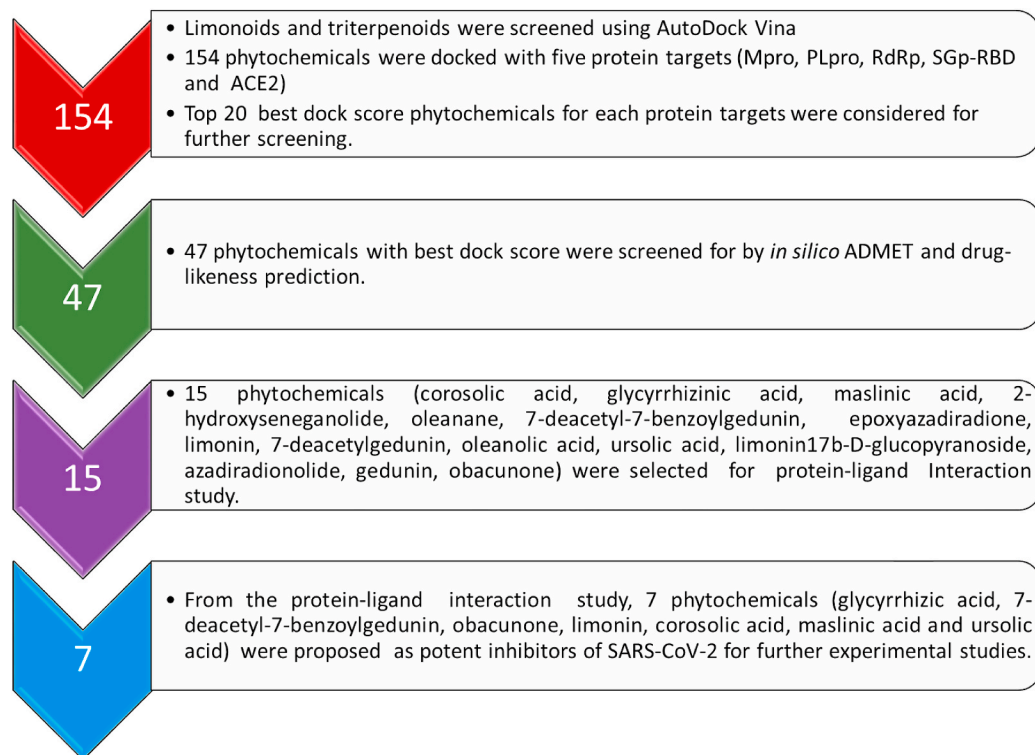
2. Experimental

2.1. Phytochemicals and proteins selection

The biologically important 154 phytochemicals from limonoids and triterpenoids were first selected based on their reported medicinal properties. The structures of the phytochemicals were collected from various sources and screened to filter the potential phytochemicals that can inhibit the effects of SARS-CoV-2. The SDF files of the selected phytochemicals were retrieved from EMBL-EBI (www.ebi.ac.uk/chebi/advancedSearchFT.do) and PUBCHEM (https://pubchem.ncbi.nlm.nih.gov/). The collected structures of the phytochemicals were further optimized by semi-empirical PM6 method coded in the computational program Gaussian 09 W [19]. The optimized structures were converted to the PDB format by using the program GaussView 5.0. The crystallography structures of the SARS-CoV-2 protein targets (3CLpro, PDB ID: 6LU7; PLpro, PDB ID: 4MM3; RdRp, PDB ID: 6M71; SGp-RDB, PDB ID: 2GHV; ACE2, PDB ID: 6M17) were retrieved from the PDB database (www.rcsb.org).

2.2. Molecular docking and simulations

The molecular docking studies were carried out to estimate the binding energies of the phytochemicals towards the therapeutic protein targets of SARS-CoV-2 by using the computational program AutoDock Vina 1.1.2 [20]. The proteins 3D structures retrieved from RCSB PDB databases were modelled using Swiss-model online server to generate

- Limonoids and triterpenoids were screened using AutoDock Vina
- 154 phytochemicals were docked with five protein targets (Mpro, PLpro, RdRp, SGp-RBD and ACE2)
- Top 20 best dock score phytochemicals for each protein targets were considered for further screening.

154

- 47 phytochemicals with best dock score were screened for by *in silico* ADMET and drug-likeness prediction.

47

- 15 phytochemicals (corosolic acid, glycyrrhizinic acid, maslinic acid, 2-hydroxyseneganolide, oleanane, 7-deacetyl-7-benzoylgedunin, epoxyazadiradione, limonin, 7-deacetylgedunin, oleanolic acid, ursolic acid, limonin17b-D-glucopyranoside, azadiradionolide, gedunin, obacunone) were selected for protein-ligand Interaction study.

15

- From the protein-ligand interaction study, 7 phytochemicals (glycyrrhizic acid, 7-deacetyl-7-benzoylgedunin, obacunone, limonin, corosolic acid, maslinic acid and ursolic acid) were proposed as potent inhibitors of SARS-CoV-2 for further experimental studies.

7

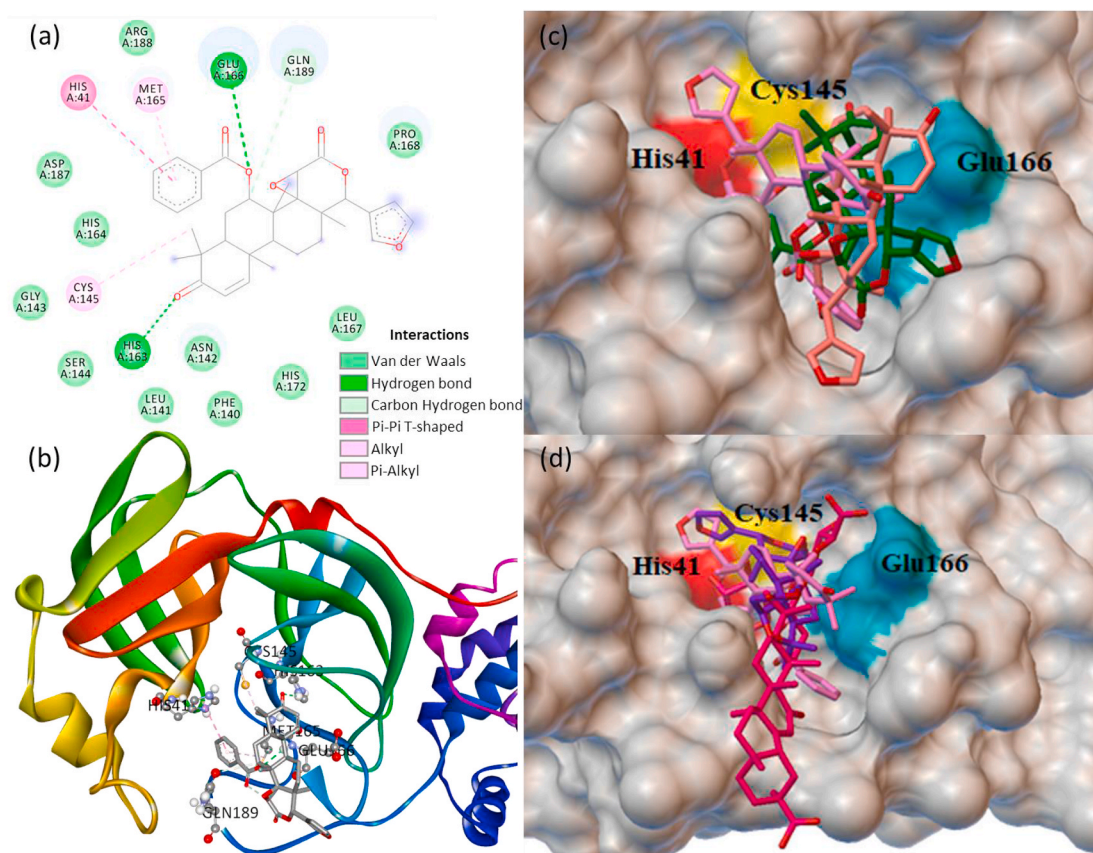**Scheme 1.** Flowchart showing the steps to screen phytochemicals for the COVID-19.

Fig. 1. (a) 2D animated pose between 7-deacetyl-7-benzoylgedunin and 3CLpro showing various non-covalent interactions, (b) 3D representation showing the position of 7-deacetyl-7-benzoylgedunin within the hydrophobic cavity of 3CLpro, (c) binding of three best poses of 7-deacetyl-7-benzoylgedunin at the active site of 3CLpro, and (d) binding of 7-deacetyl-7-benzoylgedunin, glycyrrhizic acid and limonin at the active site of 3CLpro.

Table 3
The dock score of screened phytochemicals binding at the active site of the PLpro and their important interactions with various amino acid residues.

Phytochemicals	B.E. (kcal/mole)	Important interactions at active site and catalytic triad (CYS112, HIS273, ASP287)
Obacunone	−8.3	Hydrogen bond: ARG285; Carbon Hydrogen bond: ASP287; Pi-Alkyl: HIS273, CYS271; Pi-Anion: ASP287, VDW: TRP107, THR266, GLY267, THR275, GLY272.
Glycyrrhizic acid	−8.2	Hydrogen bond: ARG285, TYR297, THR266, Carbon hydrogen bond: LYS298, GLY299, PRO300; Pi-Alkyl: HIS273, CYS271, TRP107; VDW: GLU251, GLU264, MET294, THR292, ASN110.
Ursolic acid	−7.2	Hydrogen bond: ARG285; Pi-Alkyl: HIS273, TRP107; VDW: THR275, ASP287, THR266, CYS271.
7-Deacetylgedunin	−7.1	Hydrogen bond: THR292, ARG285; Pi-Alkyl: HIS273, Pi-Sigma: HIS290; VDW: LEU291, ASP287, TRP107, THR275, THR266.

the fine structures. The missing amino acid residues (51–68, 102–110, 122–127, 895–904) were found in the crystal structure of the RdRp protein (PDB ID: 6M71). The refined protein structures were analysed by using the Ramachandran plot (Fig. S1–S5). The PDB files of the phytochemicals and proteins were converted into PDBQT format by using the AutoDock tools. The grid box dimensions and the grid map coordinates centre for the random and site specific docking for each protein were summarized in Table S1. All molecular docking studies were performed with Lamarckian genetic algorithm (LGA), and the docked structures were analysed by using the BIOVIA Discovery studio visualizer.

The protein structure flexibility and dynamics simulations were performed using the CABS-flex 2.0 online simulation tool with the default options [21]. The simulated model is generated through trajectory clustering k-medoids method. This tool calculates the protein dynamics simulations at 10 ns, predicts fluctuations and protein aggregation propensity. The root-mean-square fluctuation (RMSF) is generated based on the MD trajectory or NMR ensemble. The RMSF of a residue fluctuation profile can be calculated with the following formula:

$$RMSF = \sqrt{\frac{1}{N} \sum_{J}^{N} (x_i(j) - <x_i>)^2}$$

where, x is the residue position (Cα atom) i in the MD trajectory or NMR ensemble model j and $< >$ denotes the average over the whole MD trajectory or NMR ensemble. In CABS-flex, the statistical errors of RMSF values are reflected in root mean squared deviations (RMSD) between RMSF profile data. The CABS-flex tool detects the unusual dynamic behaviour of the secondary structure of the protein, where the higher RMSF or fluctuations during the simulation indicates the greater flexibility.

2.3. ADMET and drug-likeness prediction

After the molecular docking studies of 154 phytochemicals with the five protein targets of SARS-CoV-2, the absorption, distribution, metabolism, elimination and toxicity (ADMET) of the 47 best dock scored phytochemicals were screened using the online tool 'http://biosig.un imelb.edu.au/pkcsm/prediction' to predict their important pharmacokinetic properties. ADMET properties include absorption: Caco-2 permeability, water solubility, human intestinal absorption, P-glycoprotein substrate, P-glycoprotein I and II inhibitors, skin permeability; distribution: steady state volume of distribution (VDss), fraction unbound, blood-brain barrier (BBB) permeability, central nervous system (CNS) permeability; metabolism: cytochrome P450 inhibitors, CYP2D6/CYP3A4 substrate; excretion: renal OCT2 substrate, drug total clearance; toxicity: Rat LD50, AMES toxicity, T. pyriformis toxicity, minnow toxicity, maximum tolerated dose, oral rat chronic toxicity, hepatotoxicity, skin sensitization, hERG I and II inhibitors [22].

The drug-likeness properties were predicted using the online tool molinspiration (https://www.molinspiration.com/cgi-bin/properties) by uploading the structures of the selected phytochemicals in SMILES format. Based on the drug-likeness and bioavailability capabilities, the potential phytochemicals were finalized for further protein-ligand interaction study. It is important to mention here that the calculation of LogP is based on the formula satisfying lipophilicity, hydrophobicity and polarity of the compound, which also measure the ability of compound that could bind to the hydrophobic sites of target protein [23].

Lipophilicity = Hydrophobicity − Polarity
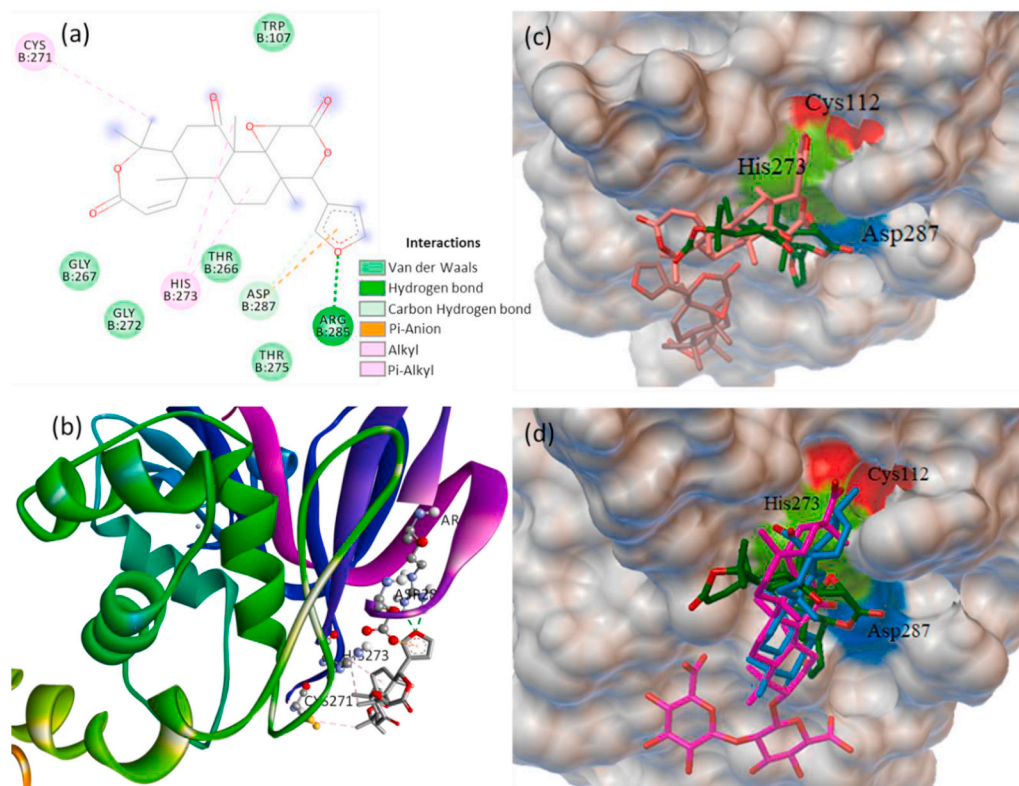LogP = aV + Λ (V = Molecular volume, Λ = Polarity term)

Fig. 2. (a) 2D animated pose between obacunone and PLpro showing various non-covalent interactions, (b) 3D representation showing the position of obacunone within the hydrophobic cavity of PLpro, (c) binding of three best poses of obacunone at the active site of PLpro, and (d) binding of obacunone, glycyrrhizic acid and ursolic acid at the active site of PLpro.

3. Results and discussion

3.1. Selection of the phytochemicals

Our recent molecular docking study on searching inhibitors for COVID-19 revealed that the phytochemical limonin known for inhibiting the replication of retroviruses like HTLV-I and HIV-1 showed the higher dock score towards the protein targets RdRp and ACE2 of SARS-CoV-2, and comparatively higher than the drug hydroxychloroquine [17]. Limonin, the highly oxygenated triterpenoid dilactone is the first isolated limonoids and till date more than 300 limonoids are isolated and characterized. The limonoids including the structural analogous triterpenoids found in medicinal plants, such as citrus, neem, tulsi and licorice, etc. are reported for various pharmaceutical properties like antiviral, antifungal, antibacterial, anticancer and antimalarial, etc., and also used routinely in the Indian traditional medicine (ayurveda) to treat various health problems [24]. The structure of limonoids and triterpenoids were first collected from the databases, i.e., EMBL-EBI and PUB-CHEM, then a basic preliminary screening of the phytochemicals were carried out based on their published medicinal importance. Total 154 phytochemicals were selected, and then studies against the five therapeutic protein targets (3CLpro, PLpro, SGp-RBD, RdRp and ACE2) of SARS-CoV-2 (Scheme 1).

3.2. Molecular docking results

The selected 154 phytochemicals were screened against the five important protein targets of SARS-CoV-2, i.e., Mpro or 3CLpro, PLpro, SGp-RBD, RdRp and ACE2 by performing random molecular docking using the computational program AutoDock Vina. The structural spike glycoprotein (S protein) of SARS-CoV-2 interacted first with the transmembrane protein of the human host cell receptor ACE2 [25,26]. This process also internalizes the virus into the endosomes, where the

conformational changes take place in the spike glycoprotein that allowed the virus to enter into the human host cell. Thereafter, the RdRp facilitates the viral genome replication [27]. The 3CLpro and PLpro act as proteases in the process of proteolysis of the viral polyprotein into functional units [28]. In short, the SGp and ACE2 are collectively involved in disease establishment and the 3CLpro, PLpro, RdRp involved in translation and replication lead to virus proliferation in the host cell. Therefore, these five proteins of SARS-CoV-2 were considered as the therapeutic protein targets for the molecular docking with the selected 154 phytochemicals.

The dock score of the 154 phytochemicals against each protein is summarized in Table S2. The table of dock score of 154 phytochemicals against the five target proteins revealed that majority of the phytochemicals showed dock score higher than −6.5 kcal/mol [29], and also comparably higher dock score than the drugs hydroxychloroquine, remdesivir and arbidol studied as a control [30]. As the core part of the structure of all phytochemicals are similar, the best 20 phytochemicals for each protein that showed higher dock score were selected for further *in silico* ADMET and drug-likeness study (Table S3).

3.3. In silico ADMET and drug-likeness results

Some phytochemicals commonly showed higher dock score with multiple protein targets and therefore, selecting best 20 phytochemicals for each protein target of SARS-CoV-2 resulted 47 phytochemicals. These 47 phytochemicals were screened further for *in silico* ADMET study and drug-likeness prediction. Out of 47, only 15 phytochemicals are obeying the ADMET limitations and drug-likeness LogP values (Table 1). These compounds satisfied the limitations of lipophilicity, hydrophobicity and polarity. The drug-likeness properties are screened based on miLogP (molinpiration LogP) values and TPSA (topological polar surface area) [31]. This study help in screening out the best phytochemical with drug-likeness and polarity of phytochemical

Table 4
The dock score of screened phytochemicals binding at the active sites of the RdRp and their important interactions with various amino acid residues.

Phytochemicals	B.E. (kcal/mole)	Important interactions at the active site (residues 611 to 626), divalent cationic residue (ASP618), catalytic site (753–767) and NTP entry channel (LYS545, ARG553, ARG555)
Glycyrrhizic acid	−9.9	Hydrogen bond: ARG624, ALA762, TRP800, ALA558, SER682, THR556, ARG555; Carbon hydrogen bond: GLY616; Pi-Alkyl: TRP800; VDW: TRP617, GLY616, ASP618, LYS798, VAL763, PHE812, ASP452, GLU811, LYS551, ASP623, VAL557, SER814, SER549, ALA547, ILE548, LYS545.
Limonin	−8.2	Hydrogen bond: TRP800, TRP617; Pi-Alkyl: CYS622, LYS798; Pi-Pi T-shaped: HIS810; VDW: PRO620, TYR619, ASP760, SER814, ASP761, ASP618, GLY616, GLU811, ALA797, LYS551
7-Deacetyl-7-benzoylgedunin	−8.2	Hydrogen bond: ALA762; Alkyl/Pi-Alkyl: LYS798; Carbon hydrogen bond: TRP617, GLU811; Pi-Anion: LYS798, Pi-Cation: ASP761, LYS551, ASP618; VDW: ALA797, TRP800, PHE812, ASP760, TYR619, PRO620.
Limonin glucoside	−8.2	Hydrogen bond: ARG624, ALA554, ARG836; Carbon hydrogen bond: SER549; Alkyl/Pi-Alkyl: HIS439, ALA550, LYS551, ARG555; VDW: ARG553, ASP452, ASP623, TYR456, SER682, VAL557, MET542, LYS545, SER814.
7-Deacetylgedunin	−8.1	Hydrogen bond: ALA762; Carbon hydrogen bond: TRP617, GLU811; Pi-Alkyl: LYS798; Pi-Sigma: TRP800; Pi-Anion: ASP761; VDW: TYR619, ASP760, ASP618, PHE812, ALA797.
Obacunone	−7.8	Hydrogen bond: LYS551, ARG624; Alkyl: ARG555; Pi-Anion: ASP452; VDW: SER549, ARG836, ALA550, ARG553, ALA554, ILE548, THR556, TYR456.

permeable in biological system. The results of ADMET properties and BOILED-Egg model of the 15 phytochemicals are summarized in Tables S4,S5, respectively. ADMET results are interpreted based on the marginal value compared with resultant value as high Caco-2 permeability predicted value > 0.90, intestinal absorption less than 30% is considered as poorly absorbed, human VDss is low if it is below 0.71 L/kg and high above 2.81 L/kg, BBB permeability logBB >0.3 considered as it cross BBB and logBB < −1 are poorly distributed. CNS permeability interpreted through logPS > −2 penetrate CNS whereas logPS < −3 unable to penetrate. T. pyriformis toxicity predicted value > −0.5 μg/L considered as toxic and minnow toxicity logLC50 < −0.3 considered as high acute toxicity [22]. Most of these potent phytochemicals finalized are found in the medicinal plants like neem, basil, licorice, olives and citrus. These 15 phytochemicals were selected for protein-ligand interaction study to identify the potential hits that bind at the active sites of the respective protein targets of SARS-CoV-2.

3.4. Protein-ligand interaction study

3.4.1. Screening of inhibitors for main protease

The main protease 3CLpro is a cysteine protease containing three domains, i.e., domains I (8–101 residues) and II (102–184 residues) with antiparallel β-barrel structure and the domain III (201–303 residues) with five α-helices linked to the domain II by a long loop (185–200 residues) [48]. The catalytic dyad CYS145 and HIS41, and the residue GLU166 involved in protein dimerization, substrate cleaving through catalysis present in the cleft between domains I and II. The enzyme active site consists of six subunits (S1–S6), and the active site residues 140–145 and 163–166 are present in the domain II. The protein-ligand

interaction study revealed that four phytochemicals (7-deacetyl-7-benzoylgedunin, glycyrrhizic acid, limonin and obacunone) bind with the catalytic dyad of 3CLpro. The dock score of the best pose of the four phytochemicals and their important molecular interactions at the active site of 3CLpro are summarized in Table 2. The 7-deacetyl-7-benzoylgedunin binds with higher dock score (−9.1 kcal/mol) at the active site followed by the glycyrrhizic acid (−8.7 kcal/mol), limonin (−8.7 kcal/mol) and obacunone (−7.5 kcal/mol).

The docked structure of 7-deacetyl-7-benzoylgedunin binds firmly at the active site of the 3CLpro long loop region of the domain II (Fig. 1a and b). The catalytic dyad CYS145 and HIS41 respectively formed Pi-alkyl and Pi-Pi T-shaped interactions. In addition, the higher binding affinity of 7-deacetyl-7-benzoylgedunin is attributed to the multiple non-covalent interactions like hydrogen bond, van der Waals (VDW) with other amino acid residues (GLU166, HIS163, ARG188, ASP187, HIS164, GLY143, SER144, LEU141, ASN142, PHE140, HIS172, LEU167, PRO168, MET165) at the active site of 3CLpro. The protein structural simulation generated RMSF graph showed the protein residues fluctuation and aggregation (Fig. S6). The fluctuated residues showing the hydrophobic cavities where substrate binding and the catalytic functions occurred. For 3CLpro simulation, the fluctuation impact at chain A residues (5–16, 46–56, 136–151, 165–178, 181–196, 241–260, 271–286), and the fluctuation impact indicating the ligand interactions at these residues. Further, the site specific docking of 7-deacetyl-7-benzoylgedunin was performed at the active site of 3CLpro, and the binding of the three best poses with the dock score of −9.1, −8.0 and −7.7 kcal/mol is shown in Fig. 1c. In addition to the 7-deacetyl-7-benzoylgedunin, the phytochemicals glycyrrhizic acid, limonin and obacunone are also binding at the active site of 3CLpro (Table 2). The binding pose of the best three phytochemicals at the active site of 3CLpro is collectively shown in Fig. 1d.

It is also important to mention here that the phytochemicals ursolic acid and oleanolic acid isolated from holy basil leaves are effectively binding at the domain III residues with the dock score of −8.9 kcal/mol, which enhanced the catalytic activity of 3CLpro. Both the phytochemicals bind with 3CLpro by forming hydrogen bonds with the residues LYS137, LEU272, and the closest non-covalent interactions with the residues THR199, ARG131 and LEU287.

3.4.2. Screening of inhibitors for PLpro

PLpro consists of four domains such as thumb, finger, palm and ubiquitin-like domain. The active site is located in between the thumb and palm domains [49]. The subunits consist of the catalytic triad (CYS112, HIS273 and ASP287), where the active site of PLpro is located. PLpro NSP3 domain contains S2/S4 inhibitor binding sites. Therefore, the molecular screening of phytochemicals that docked at specific residues of S2/S4 site could inhibit the activity of PLpro [49]. The dock score along with the important molecular interactions of the four phytochemicals (obacunone, glycyrrhizic acid, ursolic acid and 7-deacetylgedunin) binding with the catalytic triad at the active site of PLpro are summarized in Table 3. The obacunone (−8.3 kcal/mol) and glycyrrhizic acid (−8.2 kcal/mol) showed almost similar binding affinity followed by ursolic acid (−7.2 kcal/mol) at the pocket of the catalytic triad of PLpro [50,51]. In addition, the protein-ligand interaction study revealed that the phytochemicals epoxyazadiradione and limonin are also binding close to the catalytic site of PLpro.

Obacunone binds firmly at the catalytic site of PLpro, and the docked structure is stabilized by multiple non-covalent interactions (Fig. 2a and b). The catalytic residues HIS273 and ASP287 of PLpro formed Pi-alkyl and carbon hydrogen bond, respectively. Also, the obacunone formed hydrogen bond with residue ARG285, VDW contacts with TRP107, THR266, GLY267, THR275, GLY272, and Pi-alkyl interaction with CYS271. The MD simulation generated the RMSF plot of PLpro showing available contacts to substrate binding at chain B residues (5–10, 170–185, 265–270) (Fig. S7). Further, the site specific docking of obacunone was performed and the binding modes of three best poses with
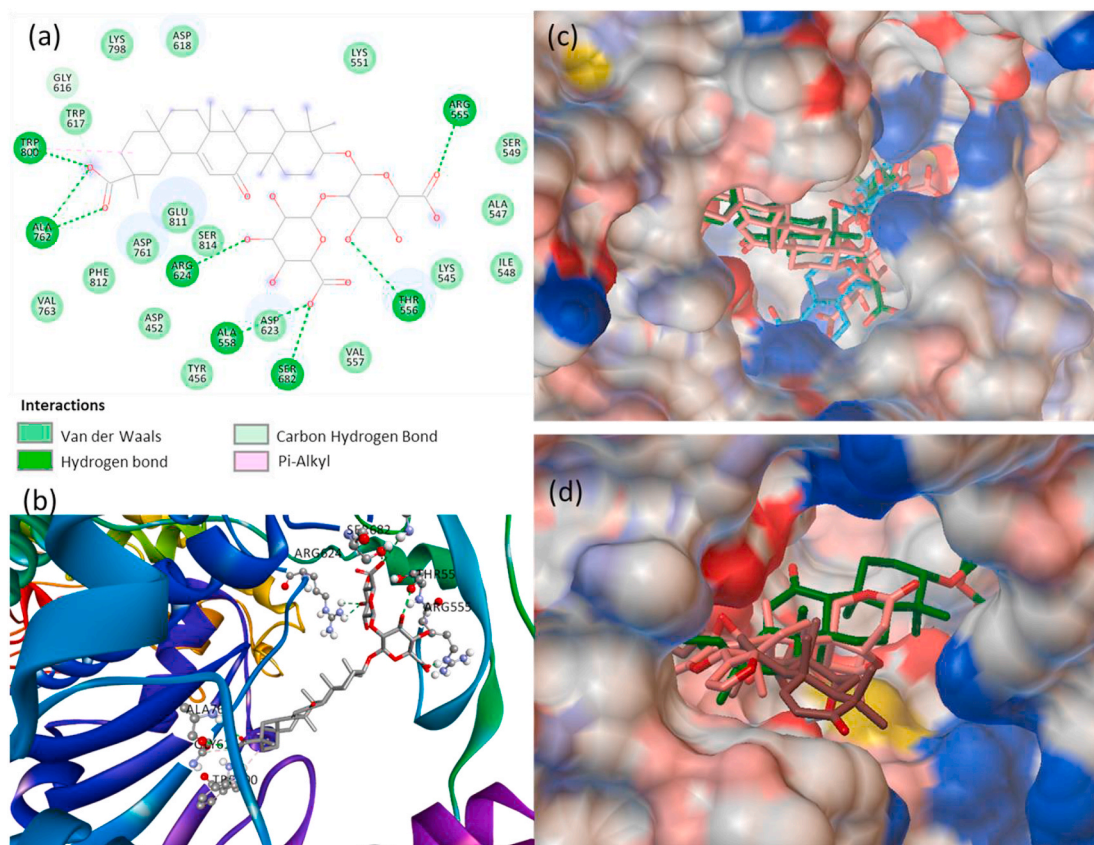
Fig. 3. (a) 2D animated pose between glycyrrhizic acid and RdRp showing various non-covalent interactions, (b) 3D representation showing the position of glycyrrhizic acid within the hydrophobic cavity of RdRp, (c) binding of three best poses of glycyrrhizic acid at the active site of RdRp, and (d) binding of glycyrrhizic acid, limonin and 7-deacetyl-7-benzoylgedunin at the active site of RdRp.

the dock score of −8.3, −7.7 and −7.3 kcal/mol at the catalytic triad of PLpro is shown in Fig. 2c. It is also important to mention here that the phytochemicals glycyrrhizic acid, ursolic acid and 7-deacetylgedunin bind with the catalytic residues HIS273 and ASP287 of PLpro. The binding modes of the best three phytochemicals at the active site of PLpro is collectively shown in Fig. 2d.

3.4.3. Screening of inhibitors for RdRp

RdRp, the non-structural protein NSP12 is a replication tool plays a major role in the transcription cycle of the virus with the help of cofactors NSP7 and NSP8. So, the primary target of the RdRp is NSP12, where the active site is located in between the NiRAN domain β-hairpin [52]. The NTP entry channel is formed by a set of hydrophilic residues such as LYS545, ARG553, and ARG555. The RdRp active site is located in the tunnel-shaped, where the protein complex posing strong electrostatic surfaces contain divalent cationic residues 611–626, especially the residue ASP618. Some catalytic residues are also located between residues 753–769. More than 80 phytochemicals bind at the RdRp functional sites, but only six phytochemicals were finalized based on their high dock score at the active site, *in silico* ADMET and drug-likeness. The interaction details and the binding energy of the six phytochemicals at the active site of RdRp are summarized in Table 4.

The best phytochemical glycyrrhizic acid is encapsulated in the receptor cavity with the maximum binding energy of −9.9 kcal/mol. The binding site is located between NiRAN domain and β-hairpin structure that polymerizes 3′ end [53], and therefore glycyrrhizic acid may interfere the polymerize activity. Glycyrrhizic acid binds firmly at the active site residues ARG624, ALA762, TRP800, ALA558, SER682, THR556, ARG555, TRP617, GLY616, ASP618, LYS798, VAL763, PHE812, ASP452, GLU811, LYS551, ASP623, VAL557, SER814,

SER549, ALA547, ILE548 and LYS545 (Fig. 3a and b). Glycyrrhizic acid formed non-covalent interaction with divalent cationic residue ASP618, hydrogen bond with ARG555 and VDW with LYS545. Also, the interactions with the catalytic residues, mainly ALA762 makes the glycyrrhizic acid potential phytochemical against RdRp. The three best binding conformations of glycyrrhizic acid at the active site of RdRp is shown in Fig. 3c, which clearly indicate that the phytochemical is well inside the hydrophobic cavity created by the residues at the active site of RdRp. Other phytochemicals limonin (−8.2 kcal/mol), 7-deacetyl-7-benzoylgedunin (−8.2 kcal/mol) and limonin glucoside (−8.2 kcal/mol) showed a similar binding affinity at the active site of RdRp. Limonin, the potent phytochemical docked at the active site between NSP12-NSP7 residues formed conventional hydrogen bonds to SER709, LYS714, ASP711, THR710, TRP800 and TRP617, and VDW interactions with residues PRO620, TYR619, ASP760, SER814, ASP761, ASP618, GLY616, GLU811, ALA797 and LYS551, including Pi-alkyl/Pi-Pi contacts with residues CYS622, LYS798 and HIS810 located in RdRp tunnel structure. The collective binding pose of the three best phytochemicals glycyrrhizic acid, limonin and 7-deacetyl-7-benzoylgedunin at the active site of RdRp is shown in Fig. 3d. Further, the MD simulations generated the RMSF plot of RdRp showing available contacts to chain A: 31–45, 255–285, 419–459, 909, chain B: 103 and 148–188 residues involved in substrate binding and replication processes (Fig. S8).

3.4.4. Screening of inhibitors for SGp-RBD

The spike protein determines the virion-host tropism that includes the entry of the virions into the host cells [54]. The receptor binding domain (RBD) of the trimeric spike glycoprotein interacts with the human host cells by binding to ACE2. Due to its structural importance, we focused on SGp-RBD inhibition study by screening 154

Table 5
The dock score of screened phytochemicals binding at the active site of the SGp-RBD and their important interactions with various amino acid residues.

Phytochemicals	B.E. (kcal/mole)	Important interactions at active site of glycosylation (ASN330, TYR356) and ACE2 binding sites (residues 438 to 527)
Maslinic acid	−9.3	Hydrogen bond: ASP454, SER456, GLY464; Pi-Alkyl: HIS445, PHE460, ARG444, PRO477, VAL458; Alkyl: PRO466; VDW: LEU443, ARG441, LYS465.
Glycyrrhizic acid	−9.3	Hydrogen bond: PHE360, ARG426, ASN427, TRP423, THR333, SER363; VDW: TYR356, ASN357, SER358, PHE361, SER362, ILE489, GLN492, ASN424, THR359, THR425, ARG495, ILE428, ASN330, ALA332.
Corosolic acid	−9.4	VDW: ASN330, PHE334, ALA331, PHE329, ARG495, TRP423, THR425, THR359, SER358, PHE360, ASN424, ASN427, TYR356, ILE428, THR332.
2-Hydroxyseneganolide	−9.2	Hydrogen bond: TRP423, VDW: ASN330, PHE329, THR359, THR425, ASN427, ASN424, SER358, TYR356, ASN357, THR332, ALA331, ARG495
Oleanane	−9.0	VDW: THR332, ALA331, TYR356, ASN330, PHE329, ARG495, TRP423, THR359, ASN424, PHE360, SER358, ASN427, THR425.
Gedunin	−8.2	Hydrogen bond: GLY368; VDW: ASP415, ASP414; Pi-Pi T-shaped: PRO399, LYS365, ALA398.

phytochemicals through molecular docking, and the binding confirmations were analysed at the active site that could inhibit the SGp-ACE2 complex formation. The RBD of the spike glycoprotein contains 333–527 residues where the active site is located [55]. The protein-ligand interaction study revealed that six phytochemicals bind at the active site, and their important molecular interactions are summarized in Table 5.

Maslinic acid binds firmly at the active site with a binding energy of −9.3 kcal/mol due to the multiple non-covalent interactions with the residues of SGp-RBD. It forms hydrogen bonds with ASP454, SER456, GLY464, alkyl/Pi-alkyl interactions with HIS445, PHE460, ARG444, PRO477, VAL458, PRO466, and VDW contacts with LEU443, ARG441, LYS465 (Fig. 4a and b). The best three binding poses of maslinic acid at the active site of SGp-RBD with the dock score of −9.3, −8.2 and −7.5 kcal/mol is shown in Fig. 4c, which revealed that this phytochemical binds with different residues at the active site of SGp-RBD. MD simulation of SpG-RBD generated the RMSF plot detailing contact sites showing the fluctuations in chain C: 432–438, 352–368, and 456–480 residues of the receptor binding site (Fig. S9). In addition to maslinic acid, the phytochemicals glycyrrhizic acid, corosolic acid, 2-hydroxyseneganolide and oleanane showed comparable binding at the active site of SGp-RBD. The binding pose of the best three phytochemicals at the active site of SGp-RBD is shown in Fig. 4d.

3.4.5. Screening of inhibitors for ACE2

ACE2 plays a key role in cardiorenal disease and acts as a human host receptor for the SARS-CoV-2 [56]. The human ACE2 receptor binds to SGp-RBD at a specific site that establishes the primary contact for host-pathogen interaction [56]. The active site residues of ACE2 were studied by using site-directed mutagenesis, and it was found that ARG273 plays a vital role in substrate binding. The HIS345 and HIS505 are catalytic residues plays an important role as a hydrogen bond donor/acceptor to form the tetrahedral peptide intermediate [57]. Also, the residues GLN24, MET82, ILE79, LYS31, HIS34, GLU37, GLY354, GLN325, ASP38, ASN330, GLU329, GLN42 and LEU45 of ACE2 receptor interact with the SGp-RBD. The protein-ligand interaction study revealed that seven phytochemicals bind at the active site of ACE2, and their important molecular interactions are summarized in Table 6. The phytochemicals glycyrrhizic acid, obacunone, azadiradionolide and gedunin bind firmly at the catalytic site of ACE2, whereas maslinic acid, epoxyazadiradione and ursolic acid binds at the RBD site of ACE2.

Glycyrrhizic acid binds firmly at the catalytic site of ACE2 with a dock score of −9.5 kcal/mol. The glycyrrhizic acid interacts to catalytic residues forming hydrogen bonds with ARG273, HIS374, TYR515, ASN394, and VDW contacts with ARG393, TYR385, GLU402, ASP350, ALA348, TRP349, ASP382, HIS505, PHE504 (Fig. 5a and b). The three best binding conformations of glycyrrhizic acid at the catalytic site of ACE2 with the dock score of −9.5, −8.3 and −8.2 kcal/mol is shown in Fig. 5c. In addition to the glycyrrhizic acid, the phytochemicals obacunone, azadiradionolide and gedunin bind to the catalytic residues ARG273, HIS345 and HIS505 with a binding energy of −8.1, −8.0 and −7.3 kcal/mol, respectively. The binding pose of the three best phytochemicals glycyrrhizic acid, obacunone and azadiradionolide at the catalytic site of ACE2 is shown in Fig. 5d. Further, the MD simulation of ACE2 complex with glycyrrhizic acid showed multiple contact sites in receptor chain B: 51–81, 141, 201–231, 261, 321–351, 531–561, 591–651 residues (Fig. S10). Out of these residues, the SGp-RBD contacts to ACE2 receptor residues GLN24, MET82, ILE79, LYS31, HIS34, GLU37, GLY354, GLN325, ASP38, ASN330, GLU329, GLN42 and LEU45. It is important to mention here that the phytochemicals maslinic acid, epoxyazadiradione and ursolic acid interact with ACE2 substrate binding site with the dock score of −8.5, −8.0 and −7.4 kcal/mol, respectively. The binding conformation of maslinic acid and epoxyazadiradione at the ACE2 substrate binding site is shown in Fig. 6. The effective binding of glycyrrhizic acid, maslinic acid, obacunone, epoxyazadiradione, azadiradionolide, ursolic acid and gedunin at the
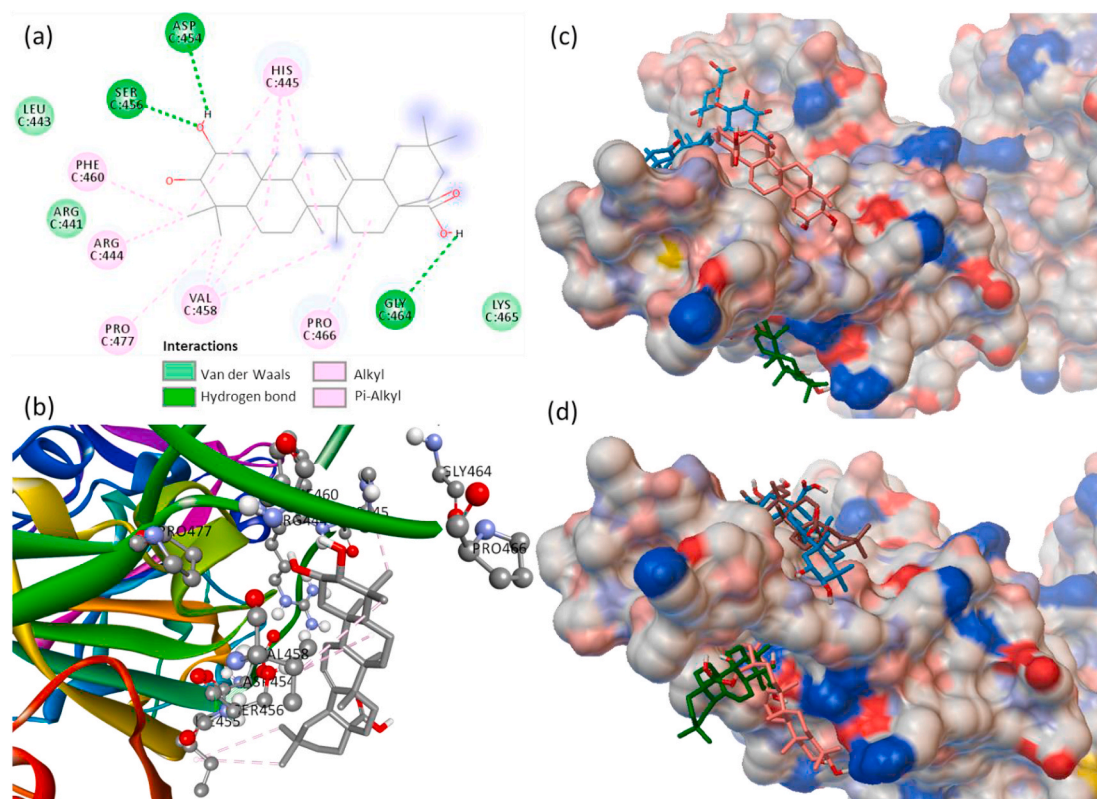
Fig. 4. (a) 2D animated pose between maslinic acid and SGp-RBD showing various non-covalent interactions, (b) 3D representation showing the position of maslinic acid within the hydrophobic cavity of SGp-RBD, (c) binding of three best poses of maslinic acid at the active site of SGp-RBD, and (d) binding of maslinic acid, glycyrrhizic acid and corosolic acid at the active site of SGp-RBD.

Table 6
The dock score of screened phytochemicals binding at the active site of the ACE2 and their important interactions with various amino acid residues.

Phytochemicals	B.E. (kcal/mole)	Important interactions at SGp-RBD docking site and catalytic sites (HIS345, HIS505 and ARG273)
Glycyrrhizinic acid	−9.5	Hydrogen bond: ARG273, HIS374, TYR515, ASN394; Pi-Alkyl: PHE40, HIS40; Carbon hydrogen bond: GLU402; VDW: ARG393, TYR385, GLU402, ASP350, ALA348, TRP349, ASP382, HIS505, PHE504.
Maslinic acid	−8.5	Hydrogen bond: PHE390, GLN388, ARG393, GLU37; Pi-Alkyl: VAL93, LYS26, PRO389; VDW: ASN33, ASP30, GLN96, THR92, ASN90.
Obacunone	−8.1	Hydrogen bond: ARG273; Pi-Sigma: PHE504; Pi-Pi T-shaped: PHE504; Pi-Alkyl: TRP271, PHE504; VDW: PHE274, GLU145, HIS505, ASN149, LEU503, TYR127, ASN508, SER128.
Epoxyazadiradione	−8.0	Alkyl/Pi-Alkyl: LYS26, PRO389; Pi-Sigma: HIS34; VDW: ASP30, ASN90, VAL93, GLN96, THR92, ASN33, GLU37.
Azadiradionolide	−8.0	Hydrogen bond: HIS345, HIS401, ASN394; Alkyl/Pi-Alkyl: HIS373, ALA348, HIS374; VDW: PHE40, TRP349, ASP350, THR347, GLU375, ARG514.
Ursolic acid	−7.4	Hydrogen bond: LYS26, ASN90, ARG393; Pi-Alkyl: VAL93, PRO389, HIS34; VDW: ASP30, THR92, GLN96, ASN33, ALA387, GLU37, PHE390.
Gedunin	−7.3	Hydrogen bond: HIS345; Alkyl/Pi-Alkyl: LUE370, PRO346, HIS374; Pi-Sigma: HIS374; Carbon hydrogen bond: PRO346; VDW: GLN442, ASP367, SER409, GLU406, GLU402, GLU375, THR371.

catalytic site and RBD site of ACE2 may potentially interfere the SGp-ACE2 complex formation, and therefore these phytochemicals can prevent the entry of the virus into the host cells.

4. Conclusions

In summary, we have screened 154 phytochemicals from limonoids and triterpenoids by molecular docking, *in silico* ADMET and drug-likeness prediction, and selected 15 phytochemicals to propose the potential hits against the five therapeutic protein targets (3CLpro, PLpro, RdRp, SpG-RBD and ACE2) of SARS-CoV-2. The phytochemicals 7-deacetyl-7-benzoylgedunin, glycyrrhizic acid, limonin and obacunone binds at the catalytic dyad of main protease 3CLpro. The phytochemicals obacunone, glycyrrhizic acid, ursolic acid and 7-deacetylgedunin binds at the catalytic triad of PLpro. Six phytochemicals glycyrrhizic acid, limonin, 7-deacetyl-7-benzoylgedunin, limonin glucoside, 7-deacetylge-dunin and obacunone are found to bind at the active site of RdRp. The SGp-RBD site is important for the virion-host tropism, where the phytochemicals maslinic acid, glycyrrhizic acid, corosolic acid, 2-hydroxy-seneganolide, oleanane and gedunin binds firmly with multiple non-covalent interactions. For the human ACE2 receptor, seven phytochemicals glycyrrhizinic acid, maslinic acid, obacunone, epoxyazadir-adione, azadiradionolide, ursolic acid and gedunin were found binding at the catalytic site and/or the RBD site. Based on the dock score and reported medicinal properties, the combination of seven phytochemicals 7-deacetyl-7-benzoylgedunin, glycyrrhizic acid, limonin, obacunone, ursolic acid, corosolic acid and masilinic acid is sufficient to formulate an appropriate therapeutic approach to fight against SARS-CoV-2. The rich sources of these phytochemicals are licorice, citrus, neem, holy basil and olives. Among the seven phytochemicals, the most important phytochemical is glycyrrhizic acid that binds at the active site of all the five protein targets of SARS-CoV-2. Overall, the computational
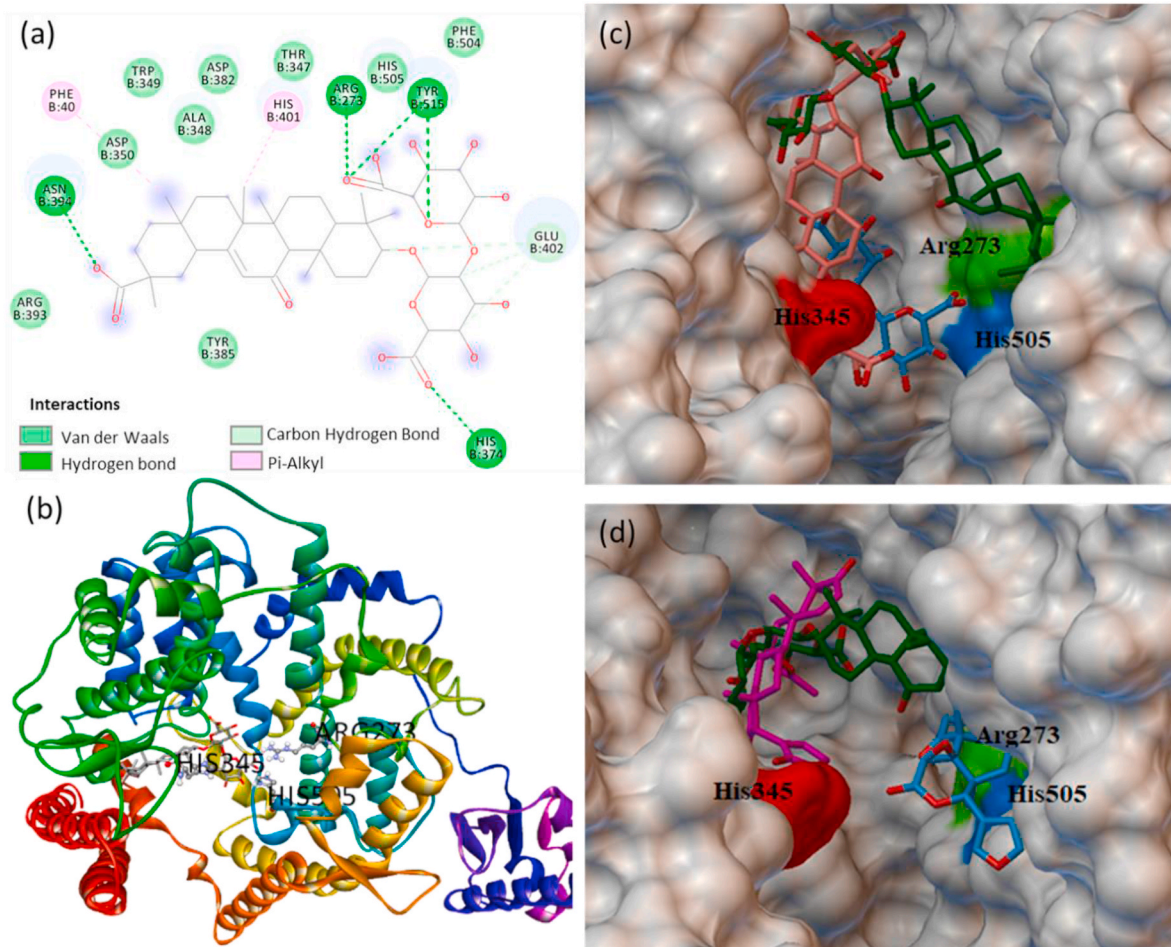
Fig. 5. (a) 2D animated pose between glycyrrhizic acid and ACE2 showing various non-covalent interactions at catalytic site and (b) the corresponding 3D representation showing binding conformation. (c) The three best poses of glycyrrhizic acid at the catalytic site of ACE2, and (d) the binding pose of three best phytochemicals glycyrrhizic acid, obacunone and azadiradionolide at the catalytic site of ACE2.
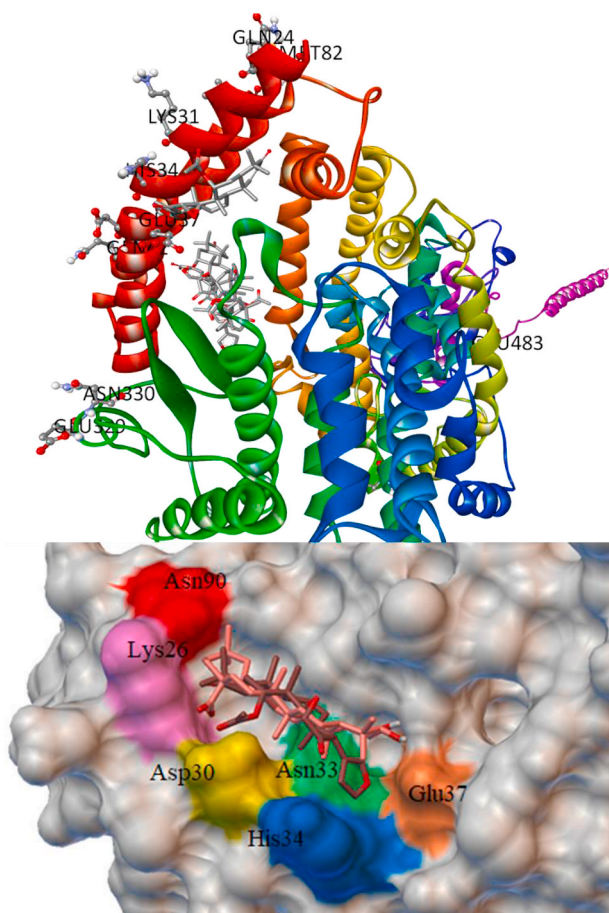
Fig. 6. The binding pose of maslinic acid and epoxyazadiradione at the RBD site of ACE2.

predictions along with the reported pharmacological properties postulated that the limonoids and triterpenoids are potential against SARS-CoV-2 target proteins. We believe the outcomes will be useful in formulating therapeutic strategies using the traditional medicines, and also the potential hits can be used for further lead optimization for drug discovery against COVID-19.

Declaration of competing interest

The authors declare that they have no known competing financial interests or personal relationships that could have appeared to influence the work reported in this paper.

Acknowledgments

Appendix A. Supplementary data

Supplementary data to this article can be found online at https://doi.org/10.1016/j.compbiomed.2020.103936.

References

[1] Y.-R. Guo, Q.-D. Cao, et al., The origin, transmission and clinical therapies on coronavirus disease 2019 (COVID-19) outbreak – an update on the status, Mil. Med. Res. 7 (2020) 11.

[2] Coronavirus Disease (COVID-2019) Situation Reports-165, 3rd July 2020, World Health Organization, 2020.

[3] https://en.wikipedia.org/wiki/Severe_acute_respiratory_syndrome_coronavirus_2.

[4] Y. Zhou, et al., Network-based drug repurposing for novel coronavirus 2019-nCoV/SARS-CoV-2, Cell Discov 6 (2020) 14.

[5] A. Singh, et al., Chloroquine and hydroxychloroquine in the treatment of COVID-19 with or without diabetes: a systematic search and a narrative review with a special reference to India and other developing countries, Diabetes Metab. Syndr. 14 (2020) 241–246.

[6] Z. Zhu, et al., Arbidol monotherapy is superior to lopinavir/ritonavir in treating COVID-19, J. Infect. 81 (2020) e21–e23.

[7] K. Choy, et al., Remdesivir, lopinavir, emetine, and homoharringtonine inhibit SARS-CoV-2 replication in vitro, Antivir. Res. 178 (2020) 104786.

[8] L. Dong, et al., Discovering drugs to treat coronavirus disease 2019 (COVID-19), Drug Discov. Ther. 14 (2020) 58–60.

[9] D. McKee, et al., Candidate drugs against SARS-CoV-2 and COVID-19, Pharmacol. Res. 157 (2020) 104859.

[10] Y. Yang, et al., Traditional Chinese medicine in the treatment of patients infected with 2019-new coronavirus (SARS-CoV-2): a review and perspective, Int. J. Biol. Sci. 16 (2020) 1708–1717.

[11] M. Liu, et al., Efficacy and safety of integrated traditional Chinese and western medicine for corona virus disease 2019 (COVID-19): a systematic review and meta-analysis, Pharmacol. Res. 158 (2020) 104896.

[12] L.T.F. Ho, et al., Highlights of traditional Chinese medicine frontline expert advice in the China national guideline for COVID-19, Eur. J. Integr. Med. 36 (2020) 101116.

[13] Y.B. Ryu, et al., SARS-CoV 3CLpro inhibitory effects of quinone-methide triterpenes from Tripterygium regelii, Bioorg. Med. Chem. Lett 20 (2010) 1873–1876.

[14] T. Pillaiyar, et al., An overview of severe acute respiratory syndrome-coronavirus (SARS-CoV) 3CL protease inhibitors: peptidomimetics and small molecule chemotherapy, J. Med. Chem. 59 (2016) 6595–6628.

[15] A.D. Fuzimoto, et al., The antiviral and coronavirus-host protein pathways inhibiting properties of herbs and natural compounds - additional weapons in the fight against the COVID-19 pandemic, J. Tradit. Complement. Med. 10 (2020) 405–419.

[16] C. Fiore, M. Eisenhut, R. Krausse, et al., Antiviral effects of Glycyrrhiza species, Phytother Res. 22 (2008) 141–148.

[17] S. Vardhan, S.K. Sahoo, Searching Inhibitors for Three Important Proteins of COVID-19 through Molecular Docking Studies, 2020 arXiv:2004.08095.

[18] H. Wang, The genetic sequence, origin, and diagnosis of SARS-CoV-2, Eur. J. Clin. Microbiol. Infect. Dis. (2020), https://doi.org/10.1007/s10096-020-03899-4.

[19] M.J. Frisch, et al., Gaussian 09W, Revision A.1, Gaussian Incorp, Wallingford, CT, 2009.

[20] O. Trott, , et al.AutoDock Vina, Improving the speed and accuracy of docking with a new scoring function, efficient optimization, and multithreading, J. Comput. Chem. (2009) 455–461.

[21] M. Jamroz, et al., CABS-flex predictions of protein flexibility compared with NMR ensembles, Bioinformatics 30 (2014) 2150–2154.

[22] D.E.V. Pires, T.L. Blundell, D.B. Ascher, pkCSM: predicting small-molecule pharmacokinetic properties using graph-based signatures, J. Med. Chem. 58 (2015) 4066–4072.

[23] https://www.sciencedirect.com/topics/immunology-and-microbiology/lipophilicity.

[24] S. Xiao, et al., Recent progress in the antiviral activity and mechanism study of pentacyclic triterpenoids and their derivatives, Med. Res. Rev. 38 (2018) 951–976.

[25] Y. Yuan, et al., Cryo-EM structures of MERS-CoV and SARS-CoV spike glycoproteins reveal the dynamic receptor binding domains, Nat. Commun. 8 (2017) 15092.

[26] J. Guy, et al., Identification of critical active-site residues in angiotensin-converting enzyme-2 (ACE2) by site-directed mutagenesis, FEBS J. 272 (2005) 3512–3520.

[27] C. Liu, et al., Research and development on therapeutic agents and vaccines for COVID-19 and related human coronavirus diseases, ACS Cent. Sci. 6 (2020) 315–331.

[28] A. Kilianski, et al., Assessing activity and inhibition of Middle East respiratory syndrome coronavirus papain-like and 3C-like proteases using luciferase-based biosensors, J. Virol. 87 (2013) 11955–11962.

[29] B. Shah, et al., In silico studies on therapeutic agents for COVID-19: drug repurposing approach, Life Sci. 252 (2020) 117652.

[30] R. Yu, et al., Computational screening of antagonists against the SARS-CoV-2 (COVID-19) coronavirus by molecular docking, Int. J. Antimicrob. Agents (2020), https://doi.org/10.1016/j.ijantimicag.2020.106012.

[31] http://www.molinspiration.com/cgi-bin/properties.

[32] J. Li, et al., Glycyrrhizic acid in the treatment of liver diseases: literature review, BioMed Res. Int. (2014) 872139.

[33] W. Yap, et al., Mechanistic perspectives of maslinic acid in targeting inflammation, Biochem. Res. Int. (2015) 279356.

[34] C. Graebin, et al., Glycyrrhizin and glycyrrhetic acid: scaffolds to promising new pharmacologically active compounds, J. Braz. Chem. Soc. 21 (2010) 1595–1615.

[35] S.A. Abdelgaleil, et al., Antifungal limonoids from the fruits of Khaya senegalensis, Fitoterapia 75 (2004) 566–572.

[36] N.R. Parikh, et al., Oleanane triterpenoids in the prevention and therapy of breast cancer: current evidence and future perspectives, Phytochem. Rev. 13 (2014) 793–810.

[37] M. Takagi, et al., Cytotoxic and melanogenesis-inhibitory activities of limonoids from the leaves of Azadirachta indica (neem), Chem. Biodivers. 11 (2014) 451–468.

[38] T. Kikuchi, et al., Cytotoxic and apoptosis-inducing activities of limonoids from the seeds of Azadirachta indica (neem), J. Nat. Prod. 74 (2011) 866–870.

[39] M. Thillainayagam, et al., Insights on inhibition of Plasmodium falciparum plasmepsin I by novel epoxyazadiradione derivatives – molecular docking and comparative molecular field analysis, J. Biomol. Struct. Dyn. 37 (2018) 3168–3182.

[40] L. Battinelli, et al., Effect of limonin and nomilin on HIV-1 replication on infected human mononuclear cells, Planta Med. 69 (2003) 910–913.

[41] R.N.C. Miranda Júnior, et al., Antiplasmodial activity of the andiroba (Carapa guianensis Aubl., Meliaceae) oil and its limonoid-rich fraction, J. Ethnopharmacol. 142 (2012) 679–683.

[42] C. Laura, et al., Oleanolic acid: a promising neuroprotective agent for cerebral ischemia, Neural. Regen. Res. 10 (2015) 540–541.

[43] A.B. Ramos-Hryb, et al., Therapeutic potential of ursolic acid to manage neurodegenerative and psychiatric diseases, CNS Drugs 31 (2017) 1029–1041.

[44] K.N.C. Murthy, et al., Citrus limonin and its glucoside inhibit colon adenocarcinoma cell proliferation through apoptosis, J. Agric. Food Chem. 59 (2011) 2314–2323.

[45] D. Kingston, et al., Modern natural products drug discovery and its relevance to biodiversity conservation, J. Nat. Prod. 74 (2011) 496–511.

[46] G. Chianese, et al., Antiplasmodial triterpenoids from the fruits of neem, Azadirachta indica, J. Nat. Prod. 73 (2010) 1448–1452.

[47] K.N.C. Murthy, et al., Obacunone and obacunone glucoside inhibit human colon cancer (SW480) cells by the induction of apoptosis, Food Chem. Toxicol. 49 (2011) 1616–1625.

[48] Z. Jin, et al., Structure of Mpro from COVID-19 virus and discovery of its inhibitors, Nature 582 (2020) 289–293.

[49] Y. Baez-Santos, et al., Catalytic function and substrate specificity of the papain-like protease domain of nsp3 from the Middle East respiratory syndrome coronavirus, J. Virol. 88 (2014) 12511–12527.

[50] Y.M. Báez-Santos, et al., The SARS-coronavirus papain-like protease: structure, function and inhibition by designed antiviral compounds, Antiviral Res 115 (2015) 21–38.

[51] N. Barretto, et al., The papain-like protease of severe acute respiratory syndrome coronavirus has deubiquitinating activity, J. Virol. 79 (2005) 15189–15198.

[52] R. Kirchdoerfer, et al., Structure of the SARS-CoV nsp12 polymerase bound to nsp7 and nsp8 co-factors, Nat. Commun. 10 (2019) 2342.

[53] Y. Gao, et al., Structure of the RNA-dependent RNA polymerase from COVID-19 virus, Science 368 (2020) 779–782.

[54] M. Letko, et al., Functional assessment of cell entry and receptor usage for SARS-CoV-2 and other lineage B betacoronaviruses, Nat. Microbiol. 5 (2020) 562–569.

[55] M. Yuan, et al., A highly conserved cryptic epitope in the receptor binding domains of SARS-CoV-2 and SARS-CoV, Science 368 (2020) 630–633.

[56] C. Rodell, et al., An ACE therapy for COVID-19, Sci. Trans. Med. 12 (2020) 541.

[57] K. Wu, et al., Crystal structure of NL63 respiratory coronavirus receptor-binding domain complexed with its human receptor, Proc. Natl. Acad. Sci. 106 (2009) 19970–19974.